frontiers | Frontiers in Physics

ORIGINAL RESEARCH
published: 03 May 2022
doi: 10.3389/fphy.2022.890865

GTPase-Dependent Mechanointegration of Shear-Mediated Cell Contractility Through Dynamic Binding of FLNa and FilGAP

L. P. Bergeron-Sandoval[1], *Alex Cai*[1,2], *Anna Clouvel*[1], *Cynthia Hitti*[1] *and Allen Ehrlicher*[1,2,3,4,5]*

[1]Department of Bioengineering, McGill University, Montreal, Canada, [2]Department of Anatomy and Cell Biology, McGill University, Montreal, Canada, [3]Rosalind and Morris Goodman Cancer Research Institute, McGill University, Montreal, Canada, [4]Department of Biomedical Engineering, McGill University, Montreal, Canada, [5]Department of Mechanical Engineering, McGill University, Montreal, Canada

Cellular mechanotransduction is a common mechanism by which cells convert mechanical cues (or stimuli) from their environment into biochemical and cellular responses. In the case of shearing forces, such as when individual cells encounter interstitial shear stress and blood shear stress, mechanotransduction involves mechanical stretching and spatial reconfiguration of Filamin A (FLNa) binding sites and subsequent release of FilGAP molecules normally bound to FLNa. However, the connection and importance of downstream molecular effectors and cellular metrics involved in response to shear stress are not understood. Here we reveal mechano-sensitive GTPase-mediated changes in cell contractility. By varying expression of FilGAP, and expression of FLNa, we show that microfluidic shear stress results in cell contractile changes only when FilGAP and FLNa dynamically bind and dissociate. By using FRET sensors that quantify the Rho or Rac charge state, we demonstrate that only cells with dynamic FLNa and FilGAP convert shear stress into GTPase activity, and the resulting downstream contractile changes. Finally, we show that manipulation of Rho and Rac through pharmacological means rescues the contractile activity, in the absence of intact FLNa-FilGAP mechanosensing. This research clarifies a precise mechanomolecular pathway used for cellular force sensing and may play critical roles in human health challenges from cancer metastasis to cardiovascular disease.

Keywords: mechanointegration, mechanotransduction, mechanocomplexes, shear stress, filamin A, FilGAP, GTPases

OPEN ACCESS

Edited by:
Liheng Cai,
University of Virginia, United States

Reviewed by:
Yinan Shen,
Harvard University, United States
Jing Xia,
Princeton University, United States

***Correspondence:**
Allen Ehrlicher
allen.ehrlicher@mcgill.ca

Specialty section:
This article was submitted to Biophysics, a section of the journal Frontiers in Physics

Received: *06 March 2022*
Accepted: *04 April 2022*
Published: *03 May 2022*

Citation:
Bergeron-Sandoval LP, Cai A, Clouvel A, Hitti C and Ehrlicher A (2022) GTPase-Dependent Mechanointegration of Shear-Mediated Cell Contractility Through Dynamic Binding of FLNa and FilGAP. Front. Phys. 10:890865. doi: 10.3389/fphy.2022.890865

INTRODUCTION

Cells *in vivo* are subjected to diverse shear stresses depending on their anatomical location [1]. In the vascular system, shear stress on the order of 1Pa caused by blood and lymph flow has been shown to regulate vasodilation and blood pressure, modulate the development and adaptation of vascular beds, and contribute to the remodeling of blood vessels [2–4]. A majority of cells are also exposed to interstitial fluid flow up to 0.1 Pa due to plasma that leaks out of capillaries to drain

into the lymphatic system [1]. Shear stress has been shown to cause cytoskeletal filament reorganization and stiffening of the cytoskeleton [3]. The ability of cells to actively respond to these mechanical forces is essential for cell homeostasis and fitness, with aberrant behavior contributing to pathology. For example, mechanical sensors and their downstream signaling factors are implicated in the regulation of cardiac contractile dysfunction and diastolic heart disease [5]. Shear stress in particular has also been shown to promote migration of breast cancer cells [1].

While mechanosensing has clear roles in physiology and pathology, the precise sensing mechanisms at the cellular level that regulate responses have remained unclear. In general, physical forces deform diverse intracellular structures, converting these mechanical stimuli into biochemical signals through a process broadly known as mechanotransduction [6]. The ability of cells to continuously detect and actively respond to these mechanical forces is mediated by an emerging group of specialized molecules called mechanosensors [7, 8].

In addition to specific structures such as stretch activated channels, the cytoskeleton itself is ideally poised to be a mechanosensor, as it is the principal generator of cellular forces, and the mechanical conductor of stress and strain [9]. One molecular mechanotransduction mechanism for shear stress involves the actin-binding protein Filamin A (FLNa). FLNa is a homodimer protein that plays important roles in cell structure and mechanosensation. FLNa is made up of an actin binding domain (ABD) and 24 repeat immunoglobulin-like domains (IGD). It can be classified into three sections, rod 1 (IGD 1–15), rod 2 (IGD 15–23), and a dimerization domain in IGD24 [10]. *Via* its ABD, FLNa crosslinks and anchors actin filaments to stabilize the plasma membrane, provide cellular cortical rigidity, and contribute to the mechanical stability of the cell [10]. FLNa also directs the formation of dynamic actin stress fibers to contribute to the shape and movement of the cell [11, 12]. Beyond its role in regulating cell structure, FLNa also forms diverse interactions with other proteins to serve as a versatile signaling scaffold. As such, FLNa may integrate external physical forces such as shear to elicit specific cellular responses. Prior work has shown that FLNa is recruited to the cell cortex in response to shear stress exposure [1]. The properties of the F-actin network are also dependent on the concentrations of FLNa [8, 13]. In response to shear force, it has been observed that F-actin networks soften at low FLNa concentrations and strain-harden at high FLNa concentrations [13]. FLNa has also been shown to play a role in tumorigenesis: in cancer cells, researchers have observed abnormal expression and subcellular localization of FLNa, suggesting it influences cytoskeleton rearrangement, migration, proliferation, and signal transduction in tumor cells [11]. For example, Filamin A-deficient human melanoma M2 cells have adhesion, motility and migration related defects and are softer than other melanoma cell lines that express FLNa [14–16]. Critically, M2 cells are insensitive to mechanical stimuli, strongly implicating FLNa as an essential mechanosensor, however, the details of this interaction have remained unclear.

Shear stress subjects the intracellular actin network to strain and deformations at the molecular level of actin associated proteins, including FLNa. It is hypothesized that as forces deform the actin cytoskeleton, FLNa's rod2 domain undergoes conformational changes to expose cryptic binding sites for signaling proteins. This changes FLNa's binding affinity for other proteins to regulate many cellular functions including motility, maintenance of cell shape, and differentiation [10]. Filamin's mechanism of mechanotransduction regulation may be linked to the more than 100 unique binding partners including integrins, kinases, and GTPases [12, 17]. One specific GTPase activating protein (GAP), FilGAP, appears to play a key role in mediating FLNa's ability to respond to shear stress.

Like other GTPases, Rac and Rho are regulated by GEFs and GAPs, which directly modulate the charge state of Rac and Rho [18–20]. FilGAP is a GAP that binds FLNa [21]. Nakamura and collaborators [22] have previously identified the binding sites that facilitate the FLNa-FilGAP interaction. Using biochemical assays, they identified that residues 723–726 in the coiled coil domain of FilGAP bind to the 23rd immunoglobulin like domain of FLNa (IGD23). Inducing a point mutation (M2474E) into IGD23 of FLNa is sufficient to abolish the FilGAP-FLNa interaction, thus FLNa M2474E does not form complexes with FilGAP. The conformation of FLNa's rod2 domain also modulates the FLNa-FilGAP interaction. Upon force generation, the rod2 domain of FLNa is deformed, reducing FLNa's binding affinity for FilGAP, and allowing the recruitment of FilGAP to the sites of membrane protrusion and force transfer where it interacts with Rac [12, 23]. At these sites, FilGAP antagonizes Rac activity to inhibit cell spreading and lamellae formation, and disruptions in the FLNa-FilGAP interaction can lead to increased force-induced apoptosis [13]. This suggests that the force-induced recruitment of FLNa and FilGAP to the cell periphery contributes to mechanoprotection [12, 24]. Several key studies from McCulloch have identified the mechanoprotective nature of FilGAP and FLNa in force mediated apoptosis, demonstrating broad importance of this mechanotransduction interaction [24–26].

FilGAP has also been shown to regulate tumor progression in glioblastoma, astrocytoma, carcinoma, and breast cancers [21, 27–29]. FilGAP promotes the mesenchymal to amoeboid transition in tumorigenesis and regulates the front-rear polarity of migrating tumor cells [28, 29]. FilGAP is thus poised to be an effective mechanosensor by regulating the relative levels of Rho and Rac activity. FilGAP directly deactivates Rac as a GAP which indirectly leads to Rho activation [21, 29, 30].

While novel upstream mechanosensors are being discovered in diverse contexts, the downstream balance of Rac and Rho activities appears to be a commonly employed biochemical switch that changes cytoskeletal activity, and in turn determines cell morphology and behavior [20]. Rac and Rho belong to the family of GTPases that regulate numerous cellular processes including actin polymerization and cell signalling [31]. The spatiotemporal coordination of Rac and Rho activity mediates cellular migration by directing the formation and organization of actin filaments. In studies using GTPase biosensors, Rho activation was observed at the leading edge of migrating cells whereas Rac activation occurred afterwards and further away from the edge, suggesting that Rho may initiate membrane protrusion

whereas Rac could promote the reinforcement and stabilization of newly formed protrusions [32]. In contradiction, another study using GTPase biosensors found that in neutrophils Rho is absent from protrusions [33].

Rac and Rho signaling also regulate the cell cycle by promoting progression through the G1 checkpoint and the formation of the mitotic spindle [31]. As Rho and Rac regulate cellular migration and proliferation, the dysregulation of their signaling may promote tumorigenesis and metastasis [34]. Although FilGAP's biochemical properties and role in cancer pathogenesis have been examined, the acute responses of FilGAP activity on biophysical activity of the cell, such as contractility under mechanical stimuli, have remained unclear. Specifically, the environmental factors that modulate cellular responses to shear stress and the characterization of Rho and Rac GTPase in contractile response to shear stress have yet to be examined. Resolving the contractile response to mechanical stimuli would thus offer a closed loop understanding of how cells physically react to changes in their environment and tune their behavior accordingly.

Here we used traction force microscopy (TFM) and Förster resonance energy transfer (FRET) to reveal that FLNa expression and dynamic FLNa-FilGAP interaction are essential for cellular response to shear stress. Using FLNa deficient cells, FLNa M2474E mutants (lacking the FilGAP binding domain), and siRNA FilGAP gene knockdown, we show that dynamic FLNa-FilGAP interactions are required to detect shear, and regulate the spatiotemporal modulation of GTPase activity, which in turn induces changes in cell contractility. By confining cells to fibronectin micropatterns, we modulated the effective shear impinging on cells, and demonstrated that cell profile and cell orientation to flow determine the timing of the cellular response. Lastly, we demonstrate the Rho pathway conservation by rescuing cell contractility through pharmacological Rho activation in cells with inhibited FLNa-FilGAP interactions. Our results cumulatively suggest that the amount of cell strain modulates the amount of FilGAP released by FLNa into the cytosol. This unbound FilGAP regulates the activity levels of RhoGTPases, and the resulting contractile response, with diverse physiological and pathological consequences.

RESULTS

We fabricated laminar flow microfluidic shear in combination with a deformable compliant lower cell substrate, allowing us to apply precisely controlled shear stress, while quantifying cell contractility using Traction Force Microscopy [35], and GTPase activity with quantitative FRET (see methods). Using this microfluidic device (**Suppplementary Figure S1A**), we imposed a 5 min flow of shear stress onto cells. We observed that FLNa expressing A7 cells display a reversible increase in contractile work (strain energy) in response to shear (**Figure 1B**). A characteristic time delay is observed for this contractile response, and cell strain energy comes back to original levels after the peak response. In FLNa-deficient M2 cells, no contractile response to shear stress is observed (**Figure 1B**).

Dynamic FLNa-FilGAP Interaction is Required for Shear Mechanosensing

To understand FLNa-dependent mechanosensing, we explored the physical and molecular underpinnings of this response within a population of Filamin A-complemented melanoma cells. We first explored the importance of the FLNa-FilGAP interaction in the cell response to shear force and assessed the impact of FLNa expression levels on shear mechanotransduction. While FLNa-deficient M2 cells displayed no mechanostimulation, transient FLNa complementation in M2 cells showed a partial recovery by demonstrating cell contractile work under shear (**Figure 1C** and **Supplementary Figure S2**). We next introduced a FLNa variant (M2474E mutation) into the M2 cells (**Supplementary Figure S2**) which has been shown to functionally crosslink actin and interact with other FLNa binding partners but lacks the binding site for FilGAP on Ig repeat 23 [22]. We observed that M2474E M2 cells are unresponsive to the applied shear stress compared to the FLNa rescue (**Figure 1C**), suggesting that FLNa's binding with FilGAP is essential for mechanotransduction. To examine if this disruption is only sensitive to changes in FLNa, we then suppressed FilGAP expression using siRNA in A7 cells (**Supplementary Figure S2**), which stably express FLNa. Cells expressing WT FLNa with downregulated FilGAP were unresponsive to external shear stress similar to cells which do not express FLNa (**Figures 1C,D**). Together these results demonstrate that both FLNa and FilGAP expression are necessary but not sufficient for mechanosensing, and that dynamic binary binding interactions are required for mechanosensing of shear stress.

Cell Contractile Response is Modulated by Cell Prestress and Shear Flow Magnitude

On the basis that cell mechanoresponse also depends on environmental factors, we next set out to determine how shear stress magnitude and substrate stiffness influence contractile response. We exposed single cells to a range of shear stress from 0.5 to 1.5 Pa; as before, no response in FLNa deficient M2 cells was observed, however, in the FLNa expressing A7 cell we observed an increase in contractile work as a function of applied shear stress (**Figures 2A,B**). To determine whether substrate material properties can impact the timing of cell response to shear, we first measured cell strain energy in response to a burst of shear in A7 cells in the main text KPa is used, in the **Figure 2C** kPa grown on PDMS substrates with a stiffness of either 10 KPa or 25 KPa. We observed that on average, cells grown on a stiffer substrate have a higher pre-shear strain energy and see a linear relationship between the prestress in the cell and the peak contractile strain energy after application of shear stress (**Figure 2C**). Since stiffer cells will deform less under an applied shear, our data suggests that cell strain is a more determinant factor than physical stress (i.e., force per area) in the cell contractile response.

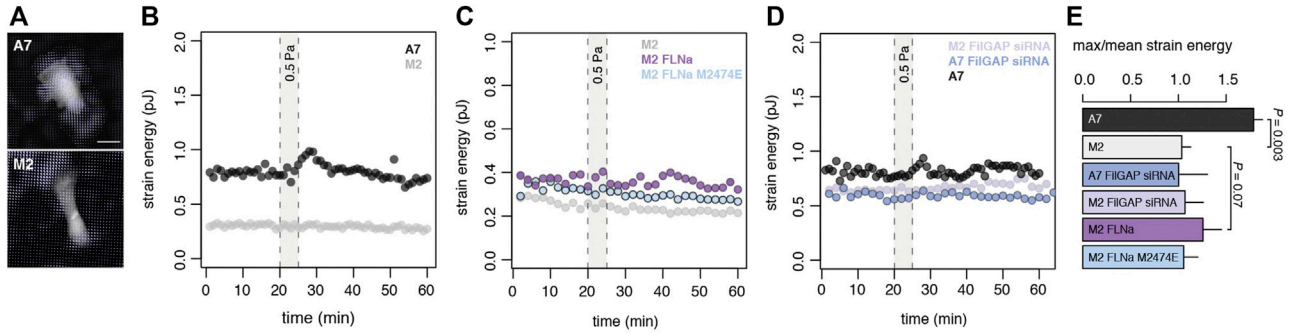

FIGURE 1 | FLNa-FilGAP interaction is necessary for mechanosensing shear **(A)** Traction stress map of A7 cells (top panel) and FLNa-null M2 cells (bottom panel) in absence of shear on time 0. Scale bar, 25 μm **(B)** Representative time series of strain energy in A7 cell (black) and M2 cell (grey). Under shear stress (5 min at 0.5 Pa) A7 cells undergo a reversible traction increase while FLNa-null M2s cell do not respond. See Panel E **(C)** Representative time series of strain energy in M2 cell (light grey) or M2 cell complemented with either mEmerald-FLNa (purple) or mEmerald-FLNa M2474E (light blue). Rescue of the contractile work is observed only in M2 mEmerald-FLNa cells when exposed to shear stress (5 min at 0.5 Pa) **(D)** Representative time series of strain energy in M2 FilGAP siRNA cell (light purple) or A7 cell (black) or A7 FilGAP siRNA cell (blue). Contractile work of A7 cells under shear is abrogated with loss of FilGAP **(E)** Maximum strain energy divided by mean strain energy for cell lines in B-D (A7 $n = 10$ cells; M2 $n = 10$ cells; A7 FilGAP siRNA $n = 3$ cells; M2 FilGAP siRNA $n = 3$ cells; M2 FLNa $n = 3$ cells; M2 FLNa M2474E $n = 3$ cells; two-sided t-test).

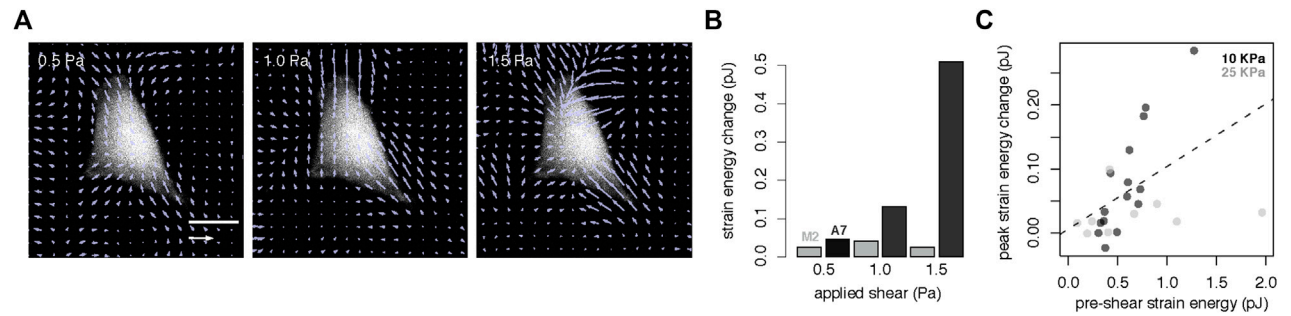

FIGURE 2 | Cell contractile response is modulated by shear flow magnitude and cell prestress **(A)** Traction stress map of example A7 cell under applied shear from 0.5 to 1.5 Pa. Scale bar, 25 μm **(B)** Change in strain energy as a function of shear for an individual A7 (black) and M2 (grey) cell **(C)** Peak strain energy change under shear (5 min at 0.5 Pa) as a function of pre-shear strain energy suggests that cells with higher prestress also display larger changes in contractility (black, 10 KPa substrate, $n =$ 15 cells; grey, 25 KPa substrate, $n = 11$ cells; dashed line, linear least squares fit).

Contractile Response Timing is Driven by Total Shear Force

The challenges of imposing varied flow rates within a single device prompted us to approach the question of varied shear force using other means, and we thus considered the varied cross-sections of cells exposed to the same shear flow to determine their individual shear forces. Using substrates of low and high stiffness, we observed similar heterogeneity for A7 cells to reach peak contractile response to shear (**Figure 3A**). Time lapse traction force microscopy at the population level also reveals an unexpected heterogeneity in peak response lag of A7 cells exposed to shear stress (**Figure 3A** and **Supplementary Figure S3**), suggesting that additional factors beyond substrate stiffness and applied stress determine response delay. We used this heterogeneity to probe the cell response to shear under constant shear regimes.

Since the effective shear force is a function of cell surface exposed to flow, we next determined if cell shape and geometry influence the timing of cell response to shear in a force dependent manner. We first quantified the profile and aspect ratio of cells exposed to shear and measured the cell contractile work. We observed that cells with lower aspect ratios respond faster than cells with higher aspect ratios (**Figure 3B**). As prior work has demonstrated that increased cell spreading flattens cells [36], our result suggests that A7 cells with low aspect ratio have a round and high profile. A high profile increases the cell cross-section exposed to the shear flow, resulting in a higher effective total shear force. Cells with high aspect ratio are also generally flatter and stiffer [36], and thus would be deformed less under the same applied stress.

Another factor that may influence the amount of cell surface exposed to shear flow is cellular orientation. We also calculated the impact of the cell major axis orientation to the shear flow on the effective shear force (**Figure 3C**). Using this approach, we noticed that randomly seeded cells exposed to a higher effective shear force have a shorter response lag than cells subject to low effective shear force (**Figure 3D**). We find an inverse linear relationship between contractile response lag and magnitude of shear stress.

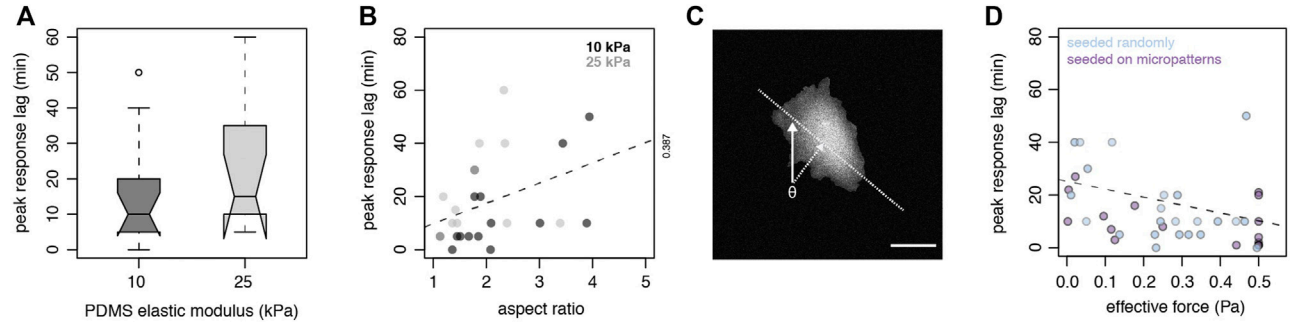

FIGURE 3 | Cell geometry, material properties and orientation to shear flow contribute to the timing of cell contractile response to shear flow **(A)** Boxplot (center line, median; box, upper and lower quartiles; whiskers, 1.5x IQR; crosses, outliers; two-sided *t*-test $p = 0.215$) of peak contractile response lag (min) to shear (5 min, 0.5 Pa) in A7 cells cultured on 10 KPa ($n = 15$ cells) or 25 KPa ($n = 11$ cells) PDMS substrates **(B)** Peak contractile response lag (min) to shear (5 min at 0.5 Pa) in randomly seeded A7 cells as a function of cell aspect ratio on 10 KPa ($n = 15$ cells) or 25 KPa ($n = 11$ cells; dashed line, linear least squares fit) **(C)** Incident angle (θ) of shear flow to cell major axis determines the *effective force* = $\sin(\theta)$ *x applied shear*. Scale bar, 25 μm **(D)** Peak contractile response lag (min) to shear (5 min at 0.5 Pa) in A7 cells as a function of effective force (Pa) of randomly seeded cells on TFM substrates (blue, $n = 26$ cells) or cells seeded on micropatterned TFM substrates (purple, $n = 21$ cells; dashed line, linear least squares fit).

Strain Heterogeneity is Regulated by Prestress and Cell Orientation

To examine more closely how cell geometry and cell orientation influence the cellular response to shear, we used fibronectin-coated micropatterns on PDMS substrates to confine cells into fixed aspect ratios and orientations to shear flow, where each pattern dictates the cell spreading (**Supplementary Figure S4**). We also determined that cell height is inversely proportional to the aspect ratio determined by cell adhesion on the fibronectin micropatterns (**Supplementary Figure S4D**).

Our TFM results on micropatterns show that the contractile response delay is also inversely proportional to the effective shear determined by the cell aspect ratio and orientation to flow (**Figure 3D**). This suggests that larger cell strains initiate faster contractile responses. Our data reinforces the idea that as forces deform the actin cytoskeleton, FLNa undergoes conformational changes to expose cryptic binding sites for signaling proteins implicated in mechanotransduction. Since dynamic binary binding interactions are required for mechanosensing, our results suggest that mechanical release of FilGAP under strain is a key step in FLNa-dependent mechanotransduction.

Strain Heterogeneity Triggers GTPase Rate Heterogeneity

Based on these observations, we next quantified FLNa-dependent mechanotransduction by probing the activity of intracellular Rac or Rho sensors. FilGAP is released from its FLNa-bound state when the cell actin network is under shear strain, making FilGAP then available to interact with and inhibit Rac [21]. The reduction in Rac activity under shear could increase the activity of the Rho pathway that stimulates actomyosin contraction [37]. To test this, we complemented cell contractility measurements with intracellular FRET-based sensors that report the charge state of Rac or Rho.

We used FRET sensors that specifically detect either Rac (Raichu-Rac1), RhoA or RhoB activity throughout the cell [38, 39]. Using a custom parallel-plate shear stress device (**Supplementary Figures S1B–C**) and the RhoA2G FRET sensor [40], we observed increased RhoA activity at the cell leading edge when cells that express FLNa are exposed to shear stress, while RhoA activity in FLNa-null cells remains unaffected by shear (**Supplementary Figure S5**). Modulation of Rho activity in time after cells are exposed to shear in a microfluidic device (**Supplementary Figure S1A**) reveals a peak of activity compared to prestress or recovery levels (**Figure 4A**).

We next performed simultaneous time-lapse analysis of traction forces, pattern deformation and Rho (DORA-RhoB sensor) activity in single cells grown on micropatterns. When cells are exposed to shear stress, we measured an increase in both cell contractility and Rho activity in FLNa complemented A7 cells (**Figure 4B**). In contrast, we observed no changes in cell contractility nor DORA-RhoB sensor activity in A7 cells in the absence of shear. FLNa deficient M2 cells show no contractile response nor RhoB activation under shear regardless of cell height or orientation to flow (**Supplementary Figure S6A**).

We also see that Rho activation speed is correlated with the magnitude of Rho signal change (**Figure 4C**). This trend is more noticeable under a high shear regime and suggests that Rho activity is strain dependent. We indeed observed that the DORA-RhoB sensor YFP/CFP ratio is significantly higher in cells exposed to an applied shear of 2.5 Pa compared to 0.5 Pa (**Figure 4D**). A proportional relationship between YFP/CFP ratio and shear is observed when we converted the applied shear into effective force (**Figure 4E**) as determined by the incident angle of flow to the cell major axis and the cell aspect ratio. These results show that Rho activation is correlated with applied shear and effective shear force, and that Rho activity is modulated by strain.

GTPase-dependent Mechanointegration of Shear-Mediated Cell Contractility

We next probed the landscape of cell contractility as a function of Rho activity to better understand how the magnitude of GTPase

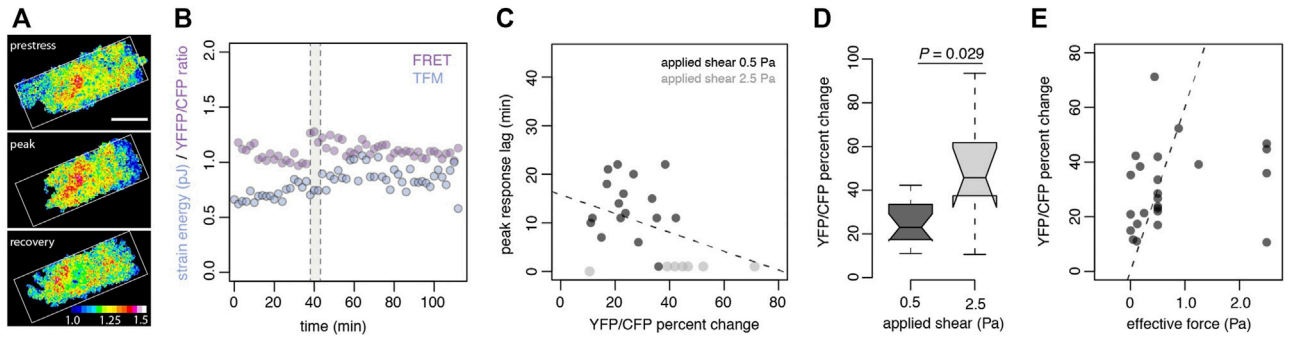

FIGURE 4 | Rho response is faster and of higher magnitude under high strain **(A)** An A7 cell stably expressing DORA-RhoB sensor on a fibronectin micropattern (white outlines; 2:1 aspect ratio rectangle, 1,000 micron^2) was exposed to shear flow to quantify prestress (top), peak (middle) and recovery (bottom) levels of DORA-RhoB activity (left panels). Scale bar, 22 μm **(B)** Representative quantification of cell contractility probed by TFM (blue) or DORA-RhoB sensor YFP/CFP ratio (purple) in A7 (n = 1 cell) exposed to shear (5 min at 0.5Pa; grey bar). No changes are observed in absence of shear or in FLNa-depleted M2 cells. **Supplementary Figure S6** **(C)** Scatterplot of peak response lag time of Dora RhoB sensor under applied shear of 0.5 Pa (black) or 2.5 Pa (grey) as a function of Dora RhoB sensor YFP/CFP ratio change. A7 cells display a faster and higher magnitude response under high strain (dashed line, linear least squares fit) **(D)** Boxplot (center line, median; box, upper, and lower quartiles; whiskers, ×1.5 IQR; crosses, outliers; two-sided t-test) of Dora RhoB sensor YFP/CFP ratio change as a function of applied shear (n = 30 cells) **(E)** Scatterplot of Dora RhoB sensor YFP/CFP ratio change as a function of controlled (cell orientation and aspect ratio) effective force (Pa) (n = 30 cells). Higher magnitude of Dora RhoB sensor YFP/CFP ratio change is observed in cells exposed to higher values of effective shear (dashed line, linear least squares fit).

signaling is coupled to actomyosin contraction. We used the time-dependent contractile response and GTPase biosensor ratios as readouts of population states. We observed that strain energy increase in A7 cells depends on Rho activation whereas Rho magnitude fluctuations are independent of the cell contractile work (**Figure 5A**). Our data suggests that while Rho is required to drive contractility it can also be decoupled from the cell contractile response. Rho is thus necessary but not sufficient for mechanoresponse. When we compared the integration of Rho sensor activity in A7 cells that respond to shear, we also observed that a characteristic threshold of total Rho activity is required for the cell to contract (**Figure 5B**). Together these results suggest that while cells need to integrate Rho activity up to a certain threshold for cell contraction, Rho activation is not a reliable predictor of a contractile response to shear. This is expected as Rho signaling regulates a number of different intracellular processes, but it also suggests that other molecular players are involved in regulating Rho-dependent shear mechanotransduction. Our observations further support the existence of contractile checkpoints that participate in the integration of external mechanical stimuli and to the overall contractile response heterogeneity.

Based on our molecular, traction and FRET data, we propose a contractile mechanism that hinges on the release and activation of FilGAP for direct inactivation of Rac and indirect activation of Rho. We next designed a pharmacological assay to confirm this idea and to control Rho and Rac activity with specific inhibitors to circumvent the absence of FLNa and trigger a contractile response in M2 cells. We successfully simulated contraction in FLNa-deficient M2 cells by combining the Rac inhibitor Ehop-16 (20 uM) [41] and the Rho agonist nocodazole (10 uM) [42] to stimulate the GTPase response and cell contraction (**Figures 5C–F**). We also reversed the GTPase and contractile responses with ROCK-inhibitor Y-27632 (10 uM) treatment (**Figures 5C,D**). These results suggest that reversible contractile work is driven by modulations in the respective Rho and Rac activity levels. To confirm that decrease of Rac activity coupled with increase of Rho activity leads to contraction, we used the same pharmacological treatment to recreate the impact of FilGAP release and activation that we observe in A7 cells under strain (**Figure 5D**). As expected, we observed an initial increase in cell traction after treatment with the combined Rac inhibitor Ehop-16 (20 uM) and the Rho agonist nocodazole (10 uM) (**Figure 5F**). We also quantified a subsequent decrease in traction after the same cell was treated with the ROCK-inhibitor Y-27632 (10 uM) (**Figure 5F**). These observations show that other drug-induced mechanoeffectors remain functional in this M2 cell in absence of FLNa. Together our results confirm that shear mechanotransduction in melanoma cells is mediated by dynamic binding of FLNa and FilGAP (**Figures 1**, **2**), the cell strain (**Figures 3**, **4**) and the modulation of Rac and Rho activities (**Figures 4**, **5**).

DISCUSSION

Mechanosensing must integrate a broad range of stimuli and draws upon diverse mechanisms. Depending on cellular and environmental context, various mechanocomplexes act as direct shear force sensors such as the Plexin D1-neuropilin 1-VEGFR system in endothelial cells [43] or the FLNa-FilGAP system [24] we studied here in melanoma cells. Mechanotransduction through the FLNa-FilGAP sensor depends on common molecular players including integrins and small GTPase. Force-dependent activation of integrins and GTPase is also a feature shared with the PECAM-1 system in endothelial cells [44].

As a mechanointegrator, the FLNa-FilGAP system convolves a broad range of stimuli and produces a breadth of responses. We

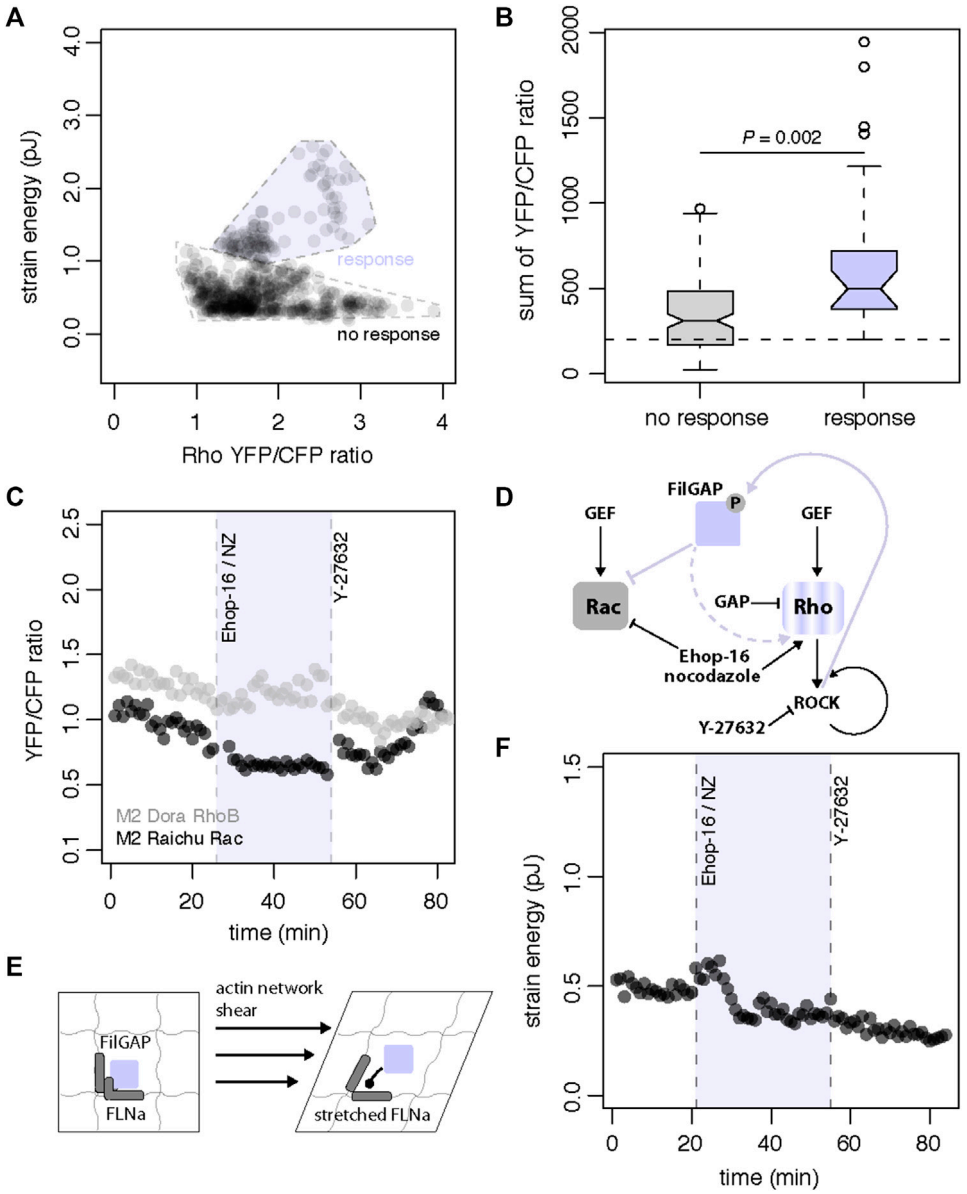

FIGURE 5 | Model of shear stress mechanosensing through FLNa-FiLGAP interaction **(A)** Landscape of strain energy in A7 cells as a function of DORA-RhoB sensor YFP/CFP ratio. High strain energy depends on DORA-RhoB sensor YFP/CFP ratio increase whereas magnitude fluctuations in DORA-RhoB sensor YFP/CFP ratio can be independent of strain energy ($n = 371$ cells) **(B)** Boxplot (center line, median; box, upper, and lower quartiles; whiskers, 1.5x IQR; crosses, outliers; two-sided *t*-test) of sum of DORA-RhoB sensor YFP/CFP ratio as a function of cell contractile response ($n = 129$ cells total). A7 cells that display a contractile response have significantly higher values for the sum of DORA-RhoB YFP/CFP ratio ($p = 0.002$) and integrate DORA RhoB sensor levels up to a characteristic threshold of YFP/CFP ratio **(C)** Time series of DORA-RhoB (grey, $n = 1$ cell) and Raichu-Rac (black, $n = 1$ cell) YFP/CFP ratios in pharmacological treatment of M2 cells with combined 20 uM Ehop-16 and 10 uM nocodazole (NZ) at 26 min and subsequent treatment with 10uM Y-27632 at 54 min **(D)** FLNa-unbound FilGAP can directly inhibit Rac and indirectly leads to cell contraction through the Rho branch. Conversely, Rac inhibitor Ehop-16 and the Rho agonist nocodazole can stimulate the GTPases response and cell contraction. The GTPases and contractile responses with ROCK-inhibitor Y-27632 treatment (arrowheads represent stimulatory modifications, flatheads represent inhibitory modifications, lines are direct modifications and dotted lines represent tentative modifications) **(E)** A molecular model of FLNa-dependent mechanotransduction. Shear stress mechanotransduction is proposed to begin through mechanical stretching and spatial reconfiguration of Filamin A (FLNa). When FLNa is stretched, it reduces the binding affinity for FilGAP and releases FilGAP in the cytosol **(F)** Time series of strain energy in pharmacological treatment of M2 cell with combined 20 μM Ehop-16 and 10 μM nocodazole at 26 min and subsequent treatment with 10 μM Y-27632 at 54 min.

observed that the delay of contractile response to shear could be predicted by the effective shear force applied to cells. Effective shear force is the deformation of cells due to shear force and is determined by cellular orientation to fluid flow and height of cell profile. This may represent a "bet-hedging" strategy used by cells to optimize the timing and magnitude of their shear response. Cells integrate many different frequencies and amplitudes of mechanical deformation from the environment; FLNa

mediated mechanosensing may use this strategy to tune their response to fluctuations in shear stress in order to maintain fitness. Indeed, we have shown that identical shear stress elicits diverse magnitudes and timing of the response; we attribute this to the varied actual resulting strain based on cell stiffness, and effective shear force. Thus, this sensitivity variation based on cell to cell geometry and alignment differences allows a collection of cells to process a broader dynamic range of stimuli than possible for a single cell's random orientation of FLNa networks [45].

Evidence for a smaller dynamic range of contractility in FLNa-complemented M2 cells reflect the importance of protein expression levels and amount of sequestered FilGAP through dynamic binding in response heterogeneity. Surprisingly, no difference in baseline Raichu-Rac activity was observed between A7 and M2 cells whereas DORA-RhoB signal is higher in M2 cells compared to A7 cells (**Supplementary Figure S7**) suggesting the existence of a feedback mechanism to control GTPases levels when the FLNa-FilGAP dynamic interaction is broken and only unbound FilGAP is present in M2 cells. FilGAP is inactive in the bound state and active in unbound state; as a result, the change in GTPase activity and contractile shear response is dampened in absence of FLNa.

FilGAP's mechanosensory role likely has broad relevance in cancer metastasis. Small GTPases have been shown to play extensive roles in regulating apical & basal polarity of individual cells, but are also crucial to regulate collective multicellular migration and fragmentation [46]. In metastatic tumor invasion FilGAP regulates polarity of breast cancer cells leading to increased migration penetration [28]. Future work will continue to resolve the extent of FilGAP mechanotransduction in diverse physiology and pathology.

MATERIALS AND METHODS

Fabrication of Soft Silicone Substrates

Compliant polydimethylsiloxane (PDMS) substrates were prepared as described by Yoshie and colleagues [47]. We obtained substrates of different modulus by mixing an equal weight ratio of PDMS components A and B (NuSil® 8100, NuSil Silicone Technologies) with respective concentrations of dimethyl siloxane-methyl hydrogen siloxane copolymer (Sylgard 184, NuSil Silicone Technologies) that effectively crosslink the PDMS. We measured with a parallel plate rheometer (Anton Paar MCR302) that PDMS substrates with weight percentage concentrations of Sylgard 184 of 0.20, 0.36 and 0.50 have Young's moduli of 5.0 ± 0.04, 12.0 ± 0.71, and 23.4 ± 1.86 kPa respectively. We laminated two layers of PDMS on 1.0 mm thick glass slides (75 × 25 mm, VWR) to obtain a uniform thickness of ~150 microns. For each layer, 0.75 ml of PDMS solution were spin coated (WS-650, Laurell Technologies) at 500 rpm for 1 min and cured at 100°C for 1 h. An additional PDMS layer with fiduciary beads was added at 2000 rpm for 1 min and cured 1 h for our traction force microscopy experiments. Substrate surfaces were functionalized with sulfo-sanpah exposed to under UV for 2 min, washed with phosphate buffered saline and incubated with fibronectin for 1 h.

Printing of Fibronectin Micropatterns for Controlled Cell Attachment

PDMS substrates were micropatterned with a UV-patterning system as described by Ghagre and collaborators [48]. PDMS substrates were incubated with 5 mg/ml poly-L-lysine (Sigma) for 30 min, washed with miliQ water and treated with 10 mg/ml polyethylene glycol valeric acid (Laysan Bio) in 0.1 M HEPES pH8.5 for 30 min. Substrates were then washed with phosphate buffered saline, covered with UV sensitive photo initiator solution (Alveole Lab) and exposed for 30 s to a patterned 29 mW/mm^2 375 nm UV laser with a Primo unit (Alveole Lab) mounted on a Ti2 eclipse microscope (Nikon) equipped with a 20x/0.45NA objective (Nikon). After the UV-based micropatterning step, the substrates were washed with phosphate buffered saline and incubated with 40 µg/ml fibronectin 5 µg/ml Alexa-555-labelled bovine serum albumin solution for 1 h. Substrates were finally washed with phosphate buffered saline and stored at 4°C prior to cell seeding.

Plasmid Preparation

mEmerald-FilaminA-N-9 plasmid (Addgene) was used to generate mEmerald-FilaminA M2474E using the GeneArt site-directed mutagenesis system (Thermo). Plasmid stocks were prepared by transforming One Shot™ TOP10 (Thermo) chemically competent *E. coli* cells, with a transformation efficiency of ~10^9 cfu/µg plasmid DNA and performing an overnight bacterial culture on kanamycin (50 µg/ml) LB Petri plates. Colonies were selected on the petri plates, and inoculation of liquid bacterial culture was done overnight in shaking incubator at 37°C. DNA was purified with QIAprep® Spin Miniprep Kit (Qiagen) and DNA was quantified with a NanoDrop spectrophotometer (Thermo).

Cell Culture, Seeding and Transfection

The human melanoma cell lines M2 and A7 cell lines were maintained in DMEM with 10% fetal bovine serum and 1% penicillin streptomycin antibiotics. Media for A7 cell lines complemented for filaminA expression also contained G418. Cell lines in filtered flasks were incubated at 37°C with 5% CO_2. Cells were seeded and incubated on fibronectin coated substrates or micropatterns for 1 h and washed with phosphate buffered saline to avoid nonspecific adhesion. Cell lines were otherwise plated onto a 6-well plate for transfection purposes. M2 cells were transfected with FLNa and FLNa M2474E using the GenJet™ DNA *In Vitro* Tranfection Reagent (SignaGen Laboratories). Cell lines with no fluorescent labels were dyed with CellTracker Green CMFDA (Invitrogen) for confocal microscopy purposes. Stable cell lines that respectively express the FRET sensors DORA-RhoB [38] and Raichu-Rac [39, 49] were generated using lentiviral transduction followed by Blasticidin selection, with codon-optimized fluorophores that prevent unwanted recombination during lentiviral gene transfer.

RNA Interference Experiments

Cells were transfected with control siRNA or siRNA oligonucleotide duplexes targeting human ARHGAP24 (siRNA ID 148940,

Thermo) using Lipofectamine® RNAiMAX Transfection Reagent (Thermo) and cultured on plastic plates for 48 h. Alternatively, cells were stably transfected with a short hairpin RNA (shRNA) against FLNa and grown in the presence of 1 g/ml puromycin.

Protein Extraction and Western Blot

Protein extraction was performed 48 h after transfection by cell lysis with ice-cold cell lysis RIPA Buffer and protein extraction protocol. Extracted proteins were stored in microcentrifuge tubes at -20°C. SDS-PAGE was performed using 4–15% Mini-PROTEAN® TGX™ precast gels (Bio-Rad) and the Mini-PROTEAN Tetra cell system (Bio-Rad) gel electrophoresis apparatus. 4X Laemmli sample buffer (Bio-Rad) was used as loading buffer. Blotting was done using the Trans-Blot® Turbo system and cassettes (Bio-Rad). Membranes were blocked with 5% bovine serum albumin (BSA) solution and primary antibody staining was performed with either 1:1,000 Filamin A monoclonal antibody (FLMN01 (PM6/317), Thermo) or 1:1,000 polyclonal mouse anti-human ARHGAP24 antibody (LS-C306327, LSBio) or 1:5,000 actin monoclonal antibody (mAbGEa, Thermo) in 1% BSA. Secondary antibody staining was done with 1:1,000 goat anti-mouse IgG (H + L)-HRP conjugate (1,706,516, Bio-Rad) in 1% BSA and imaging is done using the ChemiDoc Imaging System (Thermo). Results are processed using Image Lab Software (Bio-Rad) and ImageJ (NIH).

Confocal Microscopy

Cells on PDMS substrates were imaged on a TCS SP8 confocal microscope (Leica) equipped with a 10X/0.4NA objective (Leica) in a controlled culture environment at 37°C perfused with a 5% CO_2. We used a live cell imaging solution (Molecular Probes) for acquisition of all the fluorescence images.

Pharmalogical Treatments

For the FRET experiments we stimulated Rho activity with 5uM Nocodazole (Sigma Aldrich). We also used 10 μM Y-27632 (Sigma Aldrich) ROCK inhibitor to reduce RhoB activity. We inhibited Rac activity with 20 μM Ehop-16 (Sigma Aldrich).

Microfluidics Setup

Shear flow was applied with a μ-Slide microfluidic system (Ibidi) perfused with a syringe pump (Harvard Apparatus). μ-Slides with a channel height of 600 μm were glued over cells mounted on PDMS substrates before confocal imaging on a TCS SP8 confocal microscope and mechanical stimulation of cells unless mentioned otherwise.

Rheoconfocal Setup

We developed a customized rheometer-confocal platform to investigate the mechanical interplay between cells and shear stress. We combined a parallel plate rheometer (Anton Paar MCR302) over a TCS SP8 confocal microscope equipped with a 10X/0.4NA objective (Leica) to image cells transfected with pTriExRhoA2G (Addgene). Used for **Supplementary Figure S5** only. Sample fluorescence and interference reflection microscopy imaging was performed through a customized metal cup with a heating element and infused with 5% CO_2 (**Supplementary Figure S1**).

Live-Cell FRET Measurements

Cells mounted on PDMS substrates were stimulated and/or exposed to shear when indicated. Live-cell FRET imaging was performed on a TCS SP8 confocal microscope (Leica) equipped with a 10X/0.4NA objective (Leica). CFP was excited with a continuous wave 448 nm laser and excitation filter. Simultaneous detection of CFP (455–505 nm) and YFP (520–600 nm) channels was performed with two respective photomultiplier tubes. Images were acquired with the Leica application suite X software (Leica) and YFP/CFP ratio analysis was performed in ImageJ (NIH).

Traction Force Microscopy

Cell contractile work was measured with fiduciary beads as described previously [50]. Images of fiduciary particles in the top PDMS layer were acquired with a TCS SP8 confocal microscope (Leica) equipped with a 10X/0.4NA objective (Leica). Once the individual regions of interest with cells had been recorded, a 2% TritonX-100, 50 mM sodium azide, 500 mM potassium hydroxide solution was added prior to acquisition of the force-free reference images of the fiduciary particles. Cell strain energy were calculated with the available pyTFM script (https://github.com/fabrylab/pyTFM) based on traction force and force-free images of the fiduciary particles [35].

Pattern-Based Quantification of Cell Contractile Work

Cells' contractile work was measured with a pattern-based method as described previously [49]. The deformed and undeformed pattern areas were segmented based on fluorescent intensity threshold with ImageJ (NIH). Cell strain energies were calculated with the available MATLAB script (https://github.com/ajinkyaghagre/PaCS_156matlabcode) based on the PDMS substrate modulus and the initial pattern area.

DATA AVAILABILITY STATEMENT

The original contributions presented in the study are included in the article/**Supplementary Material**, further inquiries can be directed to the corresponding author.

AUTHOR CONTRIBUTIONS

LPB-S and AE designed the research; LPB-S and ACa performed biological research; ACl and CH performed the western blot experiments; LPB-S, ACa, and AE analyzed the biological data; LPB-S, ACa, and AE wrote the paper.

FUNDING

AE acknowledges support from NSERC (RGPIN/05843–2014, EQPEQ/472339–2015 and RTI/00348–2018),

CIHR # 143,327, and Canadian Foundation for Innovation Project #32749. LPB-S was supported by an FRQNT fellowship.

ACKNOWLEDGMENTS

The authors thank Dr Arnold Hayer for contributing four stably transfected FRET construct cell lines and his comments on the manuscript, as well as A. Ghagre and B. Guerin for technical assistance.

SUPPLEMENTARY MATERIAL

The Supplementary Material for this article can be found online at: https://www.frontiersin.org/articles/10.3389/fphy.2022.890865/full#supplementary-material

REFERENCES

1. Cole A, Buckler S, Marcucci J, Artemenko Y. Differential Roles of Actin Crosslinking Proteins Filamin and α-Actinin in Shear Flow-Induced Migration of *Dictyostelium discoideum*. *Front Cel Develop Biol* (2021) 9: 743011. doi:10.3389/fcell.2021.743011
2. Davies PF, Spaan JA, Krams R. Shear Stress Biology of the Endothelium. *Ann Biomed Eng* (2005) 33(12):1714–8. doi:10.1007/s10439-005-8774-0
3. Fletcher DA, Mullins RD. Cell Mechanics and the Cytoskeleton. *Nature* (2010) 463(7280):485–92. doi:10.1038/nature08908
4. Alonso JL, Goldmann WH. Cellular Mechanotransduction. *AIMS Biophys* (2016) 1(7):50. doi:10.3934/biophy.2016.1.50
5. Dostal DE, Feng H, Nizamutdinov D, Golden HB, Afroze SH, Dostal JD, et al. Mechanosensing and Regulation of Cardiac Function. *J Clin Exp Cardiolog* (2014) 5(6):314. doi:10.4172/2155-9880.1000314
6. Martino F, Perestrelo AR, Vinarský V, Pagliari S, Forte G. Cellular Mechanotransduction: From Tension to Function. *Front Physiol* (2018) 9: 824. doi:10.3389/fphys.2018.00824
7. Swaminathan V, Gloerich M. Decoding Mechanical Cues by Molecular Mechanotransduction. *Curr Opin Cel Biol* (2021) 72:72–80. doi:10.1016/j.ceb.2021.05.006
8. Lamsoul I, Dupré L, Lutz PG. Molecular Tuning of Filamin A Activities in the Context of Adhesion and Migration. *Front Cel Develop Biol* (2020) 8:1432. doi:10.3389/fcell.2020.591323
9. Harris AR, Jreij P, Fletcher DA. Mechanotransduction by the Actin Cytoskeleton: Converting Mechanical Stimuli into Biochemical Signals. *Annu Rev Biophys* (2018) 47(1):617–31. doi:10.1146/annurev-biophys-070816-033547
10. Razinia Z, Mäkelä T, Ylänne J, Calderwood DA. Filamins in Mechanosensing and Signaling. *Annu Rev Biophys* (2012) 41:227–46. doi:10.1146/annurev-biophys-050511-102252
11. Zhou J, Kang X, An H, Lv Y, Liu X. The Function and Pathogenic Mechanism of Filamin A. *Gene* (2021) 784:145575. doi:10.1016/j.gene.2021.145575
12. Hu J, Lu J, Goyal A, Wong T, Lian G, Zhang J, et al. Opposing FlnA and FlnB Interactions Regulate RhoA Activation in Guiding Dynamic Actin Stress Fiber Formation and Cell Spreading. *Hum Mol Genet* (2017) 26(7):1294–304. doi:10.1093/hmg/ddx047
13. Chen H, Zhu X, Cong P, Sheetz MP, Nakamura F, Yan J. Differential Mechanical Stability of Filamin A Rod Segments. *Biophysical J* (2011) 101(5):1231–7. doi:10.1016/j.bpj.2011.07.028
14. Cunningham CC, Gorlin JB, Kwiatkowski DJ, Hartwig JH, Janmey PA, Byers HR, et al. Actin-binding Protein Requirement for Cortical Stability and Efficient Locomotion. *Science* (1992) 255(5042):325–7. doi:10.1126/science.1549777
15. Flanagan LA, Chou J, Falet H, Neujahr R, Hartwig JH, Stossel TP. Filamin A, the Arp2/3 Complex, and the Morphology and Function of Cortical Actin Filaments in Human Melanoma Cells. *J Cel Biol* (2001) 155(4):511–8. doi:10.1083/jcb.200105148
16. Kim H, McCulloch CA. Filamin A Mediates Interactions between Cytoskeletal Proteins that Control Cell Adhesion. *FEBS Lett* (2011) 585(1):18–22. doi:10.1016/j.febslet.2010.11.033
17. Ithychanda SS, Qin J. Evidence for Multisite Ligand Binding and Stretching of Filamin by Integrin and Migfilin. *Biochemistry* (2011) 50(20):4229–31. doi:10.1021/bi2003229
18. Spiering D, Hodgson L. Dynamics of the Rho-Family Small GTPases in Actin Regulation and Motility. *Cell Adhes Migration* (2011) 5(2):170–80. doi:10.4161/cam.5.2.14403
19. Parri M, Chiarugi P. Rac and Rho GTPases in Cancer Cell Motility Control. *Cell Commun Signal* (2010) 8:23. doi:10.1186/1478-811x-8-23
20. Ohashi K, Fujiwara S, Mizuno K. Roles of the Cytoskeleton, Cell Adhesion and Rho Signalling in Mechanosensing and Mechanotransduction. *J Biochem* (2017) 161(3):245–54. doi:10.1093/jb/mvw082
21. Ohta Y, Hartwig JH, Stossel TP. FilGAP, a Rho- and ROCK-Regulated GAP for Rac Binds Filamin A to Control Actin Remodelling. *Nat Cel Biol* (2006) 8(8): 803–14. doi:10.1038/ncb1437
22. Nakamura F, Heikkinen O, Pentikäinen OT, Osborn TM, Kasza KE, Weitz DA, et al. Molecular Basis of Filamin A-FilGAP Interaction and its Impairment in Congenital Disorders Associated with Filamin A Mutations. *PLoS One* (2009) 4(3):e4928. doi:10.1371/journal.pone.0004928
23. Ehrlicher AJ, Nakamura F, Hartwig JH, Weitz DA, Stossel TP. Mechanical Strain in Actin Networks Regulates FilGAP and Integrin Binding to Filamin A. *Nature* (2011) 478(7368):260–3. doi:10.1038/nature10430
24. Shifrin Y, Arora PD, Ohta Y, Calderwood DA, McCulloch CA. The Role of FilGAP-Filamin A Interactions in Mechanoprotection. *MBoC* (2009) 20(5): 1269–79. doi:10.1091/mbc.e08-08-0872
25. Pinto VI, Senini VW, Wang Y, Kazembe MP, McCulloch CA. Filamin A Protects Cells against Force-induced Apoptosis by Stabilizing Talin- and Vinculin-containing Cell Adhesions. *FASEB j.* (2014) 28(1):453–63. doi:10.1096/fj.13-233759
26. Shifrin Y, Pinto VI, Hassanali A, Arora PD, McCulloch CA. Force-induced Apoptosis Mediated by the Rac/Pak/p38 Signalling Pathway Is Regulated by Filamin A. *Biochem J* (2012) 445(1):57–67. doi:10.1042/bj20112119
27. Hara A, Hashimura M, Tsutsumi K, Akiya M, Inukai M, Ohta Y, et al. The Role of FilGAP, a Rac-specific Rho-GTPase-Activating Protein, in Tumor Progression and Behavior of Astrocytomas. *Cancer Med* (2016) 5(12): 3412–25. doi:10.1002/cam4.937
28. Saito K, Mori M, Kambara N, Ohta Y. FilGAP, a GAP Protein for Rac, Regulates Front-Rear Polarity and Tumor Cell Migration through the ECM. *FASEB J* (2021) 35(4):e21508. doi:10.1096/fj.202002155R
29. Saito K, Ozawa Y, Hibino K, Ohta Y. FilGAP, a Rho/Rho-Associated Protein Kinase-Regulated GTPase-Activating Protein for Rac, Controls Tumor Cell Migration. *MBoC* (2012) 23(24):4739–50. doi:10.1091/mbc.e12-04-0310
30. Nakamura F. FilGAP and its Close Relatives: a Mediator of Rho-Rac Antagonism that Regulates Cell Morphology and Migration. *Biochem J* (2013) 453(1):17–25. doi:10.1042/bj20130290
31. Jaffe AB, Hall A. Rho GTPases: Biochemistry and Biology. *Annu Rev Cel Dev. Biol.* (2005) 21:247–69. doi:10.1146/annurev.cellbio.21.020604.150721
32. Machacek M, Hodgson L, Welch C, Elliott H, Pertz O, Nalbant P, et al. Coordination of Rho GTPase Activities during Cell Protrusion. *Nature* (2009) 461(7260):99–103. doi:10.1038/nature08242
33. Yang HW, Collins SR, Meyer T. Locally Excitable Cdc42 Signals Steer Cells during Chemotaxis. *Nat Cel Biol* (2016) 18(2):191–201. doi:10.1038/ncb3292
34. Sanz-Moreno V, Marshall CJ. Rho-GTPase Signaling Drives Melanoma Cell Plasticity. *Cell Cycle* (2009) 8(10):1484–7. doi:10.4161/cc.8.10.8490
35. Bauer A, Prechová M, Fischer L, Thievessen I, Gregor M, Fabry B. pyTFM: A Tool for Traction Force and Monolayer Stress Microscopy. *Plos Comput Biol* (2021) 17(6):e1008364. doi:10.1371/journal.pcbi.1008364

36. Guo M, Pegoraro AF, Mao A, Zhou EH, Arany PR, Han Y, et al. Cell Volume Change through Water Efflux Impacts Cell Stiffness and Stem Cell Fate. *Proc Natl Acad Sci U S A* (2017) 114(41):E8618–E27. doi:10.1073/pnas.1705179114
37. Wozniak MA, Desai R, Solski PA, Der CJ, Keely PJ. ROCK-generated Contractility Regulates Breast Epithelial Cell Differentiation in Response to the Physical Properties of a Three-Dimensional Collagen Matrix. *J Cel Biol* (2003) 163(3):583–95. doi:10.1083/jcb.200305010
38. Reinhard NR, van Helden SF, Anthony EC, Yin T, Wu YI, Goedhart J, et al. Spatiotemporal Analysis of RhoA/B/C Activation in Primary Human Endothelial Cells. *Sci Rep* (2016) 6:25502. doi:10.1038/srep25502
39. Komatsu N, Aoki K, Yamada M, Yukinaga H, Fujita Y, Kamioka Y, et al. Development of an Optimized Backbone of FRET Biosensors for Kinases and GTPases. *MBoC* (2011) 22(23):4647–56. doi:10.1091/mbc.e11-01-0072
40. Fritz RD, Letzelter M, Reimann A, Martin K, Fusco L, Ritsma L, et al. A Versatile Toolkit to Produce Sensitive FRET Biosensors to Visualize Signaling in Time and Space. *Sci Signal* (2013) 6(285):rs12. doi:10.1126/scisignal.2004135
41. Autenrieth TJ, Frank SC, Greiner AM, Klumpp D, Richter B, Hauser M, et al. Actomyosin Contractility and RhoGTPases Affect Cell-Polarity and Directional Migration during Haptotaxis. *Integr Biol (Camb)* (2016) 8(10):1067–78. doi:10.1039/c6ib00152a
42. Chang Y-C, Nalbant P, Birkenfeld J, Chang Z-F, Bokoch GM. GEF-H1 Couples Nocodazole-Induced Microtubule Disassembly to Cell Contractility via RhoA. *MBoC* (2008) 19(5):2147–53. doi:10.1091/mbc.e07-12-1269
43. Mehta V, Pang K-L, Rozbesky D, Nather K, Keen A, Lachowski D, et al. The Guidance Receptor Plexin D1 Is a Mechanosensor in Endothelial Cells. *Nature* (2020) 578(7794):290–5. doi:10.1038/s41586-020-1979-4
44. Collins C, Guilluy C, Welch C, O'Brien ET, Hahn K, Superfine R, et al. Localized Tensional Forces on PECAM-1 Elicit a Global Mechanotransduction Response via the Integrin-RhoA Pathway. *Curr Biol* (2012) 22(22):2087–94. doi:10.1016/j.cub.2012.08.051
45. Kang J, Puskar KM, Ehrlicher AJ, LeDuc PR, Schwartz RS. Structurally Governed Cell Mechanotransduction through Multiscale Modeling. *Sci Rep* (2015) 5(1):8622. doi:10.1038/srep08622
46. Zegers MM, Friedl P. Rho GTPases in Collective Cell Migration. *Small GTPases* (2014) 5:e28997. doi:10.4161/sgtp.28997
47. Yoshie H, Koushki N, Kaviani R, Tabatabaei M, Rajendran K, Dang Q, et al. Traction Force Screening Enabled by Compliant PDMS Elastomers. *Biophysical J* (2018) 114(9):2194–9. doi:10.1016/j.bpj.2018.02.045
48. Ghagre A, Amini A, Srivastava LK, Tirgar P, Khavari A, Koushki N, et al. Pattern-Based Contractility Screening, a Reference-free Alternative to Traction Force Microscopy Methodology. *ACS Appl Mater Inter* (2021) 13(17):19726–35. doi:10.1021/acsami.1c02987
49. Bisaria A, Hayer A, Garbett D, Cohen D, Meyer T. Membrane-proximal F-Actin Restricts Local Membrane Protrusions and Directs Cell Migration. *Science* (2020) 368(6496):1205–10. doi:10.1126/science.aay7794
50. Yoshie H, Koushki N, Molter C, Siegel PM, Krishnan R, Ehrlicher AJ. High Throughput Traction Force Microscopy Using PDMS Reveals Dose-dependent Effects of Transforming Growth Factor-β on the Epithelial-To-Mesenchymal Transition. *J Vis Exp* (2019) 148:59364. doi:10.3791/59364

Conflict of Interest: The authors declare that the research was conducted in the absence of any commercial or financial relationships that could be construed as a potential conflict of interest.

Publisher's Note: All claims expressed in this article are solely those of the authors and do not necessarily represent those of their affiliated organizations, or those of the publisher, the editors and the reviewers. Any product that may be evaluated in this article, or claim that may be made by its manufacturer, is not guaranteed or endorsed by the publisher.